Supplementary Information

~~Boosting Loading Capacities of Shapeable MOFs as Solid-Phase Microextraction Coatings by Closing the Interparticle Spaces of Stacked Nanocrystals~~Boosting Loading Capacities of Shapeable Metal-Organic Framework Coatings by Closing the Interparticle Spaces of Stacked Nanocrystals

Songbo Wei[†], Yan Liu[†], Jiating Zheng[†], Siming Huang[‡], Guosheng Chen[†], Fang Zhu[†], Juan Zheng[a], Jianqiao Xu*[,†], Gangfeng Ouyang*[,†]

[†]MOE Key Laboratory of Bioinorganic and Synthetic Chemistry/KLGHEI of Environment and Energy Chemistry, School of Chemistry, Sun Yat-sen University, Guangzhou 510275, China.

[‡]Department of Radiology, Sun Yat-sen Memorial Hospital, Sun Yat-sen University, Guangzhou 510120, Guangdong, China

Text S1. Chemicals. All chemicals were used as purchased without any purification. Cupric nitrate (≥98%), 1,3,5–benzentricarboxylate (BTC, 95%) and imidazole (99%) were obtained from Aladdin Chemistry Co., Ltd. (Shanghai, China). Ethanol (≥99.7%), acetone (A.R.) and methanol (A.R.) were purchased from Guangzhou Chemical Reagents Company. Polydimethylsiloxane (PDMS) stamp was prepared using the SYLGARD 184 silicone elastomer kit from Dow Corning (Shanghai, China) and following the official instruction. Commercial PDMS fiber (30 μm) was purchased from Supelco (Bellefonte, United States). Zinc nitrate hexahydrate was purchased from Sigma-Aldrich (Shanghai, China). Stainless steel wires (SSWs, 127 μm) were acquired from Small Parts (Miami Lakes, United States). Six polycyclic aromatic hydrocarbons (PAHs) pollutants (P1, acenaphthene; P2, fluorene; P3, phenanthrene; P4, anthracene; P5, fluoranthene; P6, pyrene) were purchased from Dr. Ehrenstorfer GmbH (Germany).

Text S2. Synthesis of monolithic HKUST-1 ($_{mono}$HKUST-1) and silicone-coated $_{mono}$HKUST-1 ($_{Simono}$HKUST-1) samples. This process was based on the modifications of a reported method.[1] Using ethanol as solvent, BTC solution (10 ml, 0.061 M) and Cupric nitrate solution (10 ml, 0.063M) were combined and stirred for 10 min at 25 ±1 °C. After being centrifuged, the yielded solid was washed and ultrasonicated in ethanol for 10 min (4 ml, 4 times) and then dried in an oven at 25 ±1 °C for 12 h. The solid was shifted to a petri dish and was further dried at 120 °C under vacuum for another 12 h.

To obtain $_{Simono}$HKUST-1, a PDMS stamp (5 cm in diameter) was prepared on the lid of the petri dish. The solid was spread over the base of the petri dish. Finally, the base was capped with the PDMS-loaded lid, and heated at 250 °C for 60 min.

Text S3. Synthesis of powder HKUST-1 ($_{powd}$HKUST-1) and silicone-coated $_{powd}$HKUST-1 ($_{Sipowd}$HKUST-1) samples. This process was similar to that of $_{Simono}$HKUST-1. The only difference is that after the solid was washed and ultrasonicated in ethanol for 10 min (4ml, 3 times), rather than being dried at room temperature, it was dried at 120 °C for 12 h.

Text S4. Synthesis of powder ZIF-8 ($_{powd}$ZIF-8) and monolithic ZIF-8 ($_{mono}$ZIF-8) samples. This process was based on the literature.[2,3] Using ethanol as solvent, $Zn(NO_3)_2$•$6H_2O$ (20 mL, 0.99 mmol) solution was rapidly poured into Hmim solution (20 mL, 7.904 M) under stirring with a magnetic bar for 3 h at room temperature. After centrifugation, the collected solid was washed in ethanol (15 ml, 4 times) under ultrasonication for 180 s. The solid was processed with two different approaches to obtain either $_{powd}$ZIF-8 or $_{mono}$ZIF-8. Specifically, $_{powd}$ZIF-8 was obtained by drying the solid at 120 °C overnight in a vacuum oven. $_{mono}$ZIF-8 was obtained by drying the solid at room temperature overnight followed by the subsequent evacuation of moistures at 120 °C in the vacuum oven for 2 h.

Text S5. Fabrication of the $_{Sipowd}$HKUST-1 coating and the $_{powd}$ZIF-8 coating. This process was similar to what was adopted in our previous work[4]. All SSWs were processed with the following procedures. Briefly, a 3-cm-long SSW was ultrasonicated in methanol (15 min) and subsequently in acetone (15 min). 0.5 g of PDMS was dissolved and ultrasonicated in 1.5 mL *o*-xylene, which was used as the gluing agent. A drop of the gluing agent was placed on a Kimwipes tissue (Kimberly-Clark). The clean SSW was wiped with the tissue to be covered with an adhesive thin layer of silicone. To obtain a $_{powd}$ZIF-8 SPME coating, an SSW was rolled back and forth in the solid of $_{powd}$ZIF-8 and the excessive solid on the SSW was gently blown away with a rubber suction bulb. Similarly, to obtain the $_{Sipowd}$HKUST-1 coating, an SSW was rolled back and forth in the solid of $_{Sipowd}$HKUST-1. The coatings were aged at 250 °C for 30 min before use.

Text S6. Fabrication of the $_{mono}$HKUST-1 coating, the $_{mono}$ZIF-8 coating and the $_{Simono}$HKUST-1 coating. All SSWs were ultrasonicated in methanol (15 min) and subsequently in acetone (15 min). Then, they were etched in *aqua regia* (hydrochloric acid: nitric acid = 3: 1) for 45 s to increase surface roughness. Washed by deionized (DI) water, the SSWs were immersed in ethanol for another 1 h and placed at 50 °C to dry off. The yielded HKUST-1 wet gel was dissolved in 3 mL ethanol to form a dense solution. As shown in Scheme S1a, the solution was pumped into a hollow borosilicate glass capillary by a syringe (Scheme S1a). Then a pretreated SSW was inserted into the loaded capillary and dried off at room temperature for 24 h to yield a cylindrical $_{mono}$HKUST-1 SPME coating. Then, the borosilicate glass capillary was chipped away with great care using a tweezer. The coating was heated at 120 °C for 12 h for activation.

The $_{mono}$ZIF-8 coating was prepared with the same method, except that the precursor was $_{mono}$ZIF-8.

To improve moisture resistance, the cylindrical $_{mono}$HKUST-1 coating was placed in a PDMS-loaded vial and heated at 250 °C for 1 h to yield the $_{Simono}$HKUST-1 coating (Scheme S1b).

Text S7. Characterizations. Powder X-ray diffraction (PXRD) patterns were obtained using a Bruker D8 Advance diffractometer (Germany). Scanning electron microscope (SEM) images were taken by an SU8010 ultra-high-resolution field emission SEM (Hitachi, Japan). Transmission electron microscope (TEM) images were taken from a FEI Tecnai G2 Spirit TEM (FEI, Netherlands) with a voltage of 120 kV. X-ray photoelectron spectra were obtained from an X-ray photoelectron spectrometer (XPS, ESCALab 250) using monochromatic Al kα radiation (1486.6 eV) as the excitation source. Functional group analysis was conducted on a PerkinElmer Fourier transform infrared (FT-IR) spectrometer. Elemental analysis (EA) was carried out using Elementar Vario EL (Germany) for the analysis of C, H, N. A GC-MS (7890-5975C) system equipped with an HP-5MS capillary column (30 m × 0.25 mm × 0.25μm) (Agilent Technologies, USA) was employed for the separation and quantification of PAHs. An MPS (GERSTEL, Germany) was used for automated sampling. True density measurement was carried out with a TD-2200 true density analyzer (Beijing Builder Electronic Technology, China). Thermogravimetric (TG) data were collected from a TG 209 F3 Tarsus thermogravimetry (Netzsch, Germany). Brunauer–Emmett–Teller (BET) area was obtained based on the BET theory with the aid of a Micrometrics ASAP 2020 analyzer.

Contact angle was obtained from a DSA100 drop shape analyzer (Kruss, Germany). Specifically, using a motor-driven syringe, the water droplet (less than 10 μL) was slowly added to the surface of the samples and captured by the camera system attached to the analyzer. All sessile water contact angle measurements were carried out under ambient temperature (*i.e.,* ~25 ^{o}C).

Text S8. Density measurement of $_{mono}$HKUST-1 (or $_{mono}$ZIF-8). Density measurement was based on Archimedes' principle using a similar approach in the lieterature.[1] First of all, the $_{mono}$HKUST-1 (or $_{mono}$ZIF-8) sample was weighed. Then, it was gently immersed in a 5 mL cylinder filled with 3 mL silicone oil. The subsequent increase of the liquid height was observed and recorded. The volume difference between the cylinders before and after the monolith was immersed was equal to the volume of the monolith. All the measurements were conducted in triplicate in order to reduce accidental error.

Text S9. Direct immersion SPME (DI-SPME). All the experiments were performed in triplicate. First of all, a coating was aged at 250 °C for 30 min before use. PAHs water samples (that is, certain concentrations of PAHs dissolved in 10 ml of deionized water) in 10-ml vials were placed

on the sample tray followed by the automatic extraction and analysis *via* a multi-purpose sampler (MPS) and gas chromatography-mass spectrometry (GC-MS).

Text S10. Optimization of Extraction and Desorption Conditions. Experimental conditions were optimized, including extraction time and temperature, desorption temperature and salt concentration (ionic strength). To optimize extraction time, the other three parameters were kept constant (*i.e.*, extraction time as 40 min, desorption temperature as 250 °C, no salt was added in the aqueous solutions). A series of sample solutions were prepared and extracted at temperatures from 30 to 70 °C. Similarly, the other three parameters were optimized.

Conditions like extraction time, extraction temperature, desorption temperature and ionic strength were optimized (Figure S11).

First, a series of extraction experiments were conducted at 40 °C to optimize the extraction time. The extraction time profile showed that extraction efficiency hit maximum at 60 min and plateaued afterwards, which suggested that the extraction process reached equilibrium after 60 min of extraction at 40 °C. Thus, the extraction time of 60 min was chosen. Second, a series of samples were extracted for 60 min at different temperatures to explore the optimal extraction temperature. Extraction efficiency increased as extraction temperature rose from 30 to 40 °C and then decreased as the temperature continued to go up until 70 °C. The extraction temperature profile showed the maximum extraction efficiency at 40 °C, so it was chosen as the optimal extraction temperature. Third, a series of samples were extracted at 40 °C for 60 min and then desorbed at different temperatures to draw a desorption temperature profile. The profile showed an increase of desorption efficiency until 250 °C and then plateaued after that. Therefore, 250 °C was selected as the optimal desorption temperature. Finally, ionic strength, which could be adjusted by salt addition, was optimized. The salt concentration profile displayed a plateau followed by a decrease of the extraction efficiency, so the following experiments were carried out without salt addition. Traditionally, an increase in ionic strength is able to result in an improvement of extraction efficiency in most cases. However, for analytes with constant aqueous solubility, as in this case, change in ionic strength would reduce the partition coefficients between the analytes and the SPME coating.

In summary, optimization conditions were, extraction time was 60 min; extraction temperature was 40 ℃; desorption temperature was 250 ℃; no salt was added.

Text S11. Discussion of the PDMS layer at the surface of $_{\text{Simono}}$HKUST-1. At 250 °C, the PDMS stamp broke into shorter and more volatile species to form a nanoscale conformal shield on the surface of the $_{\text{mono}}$HKUST-1 coating.[5] The compositional silicon species of the original PDMS sources were different from those at the surface of $_{\text{Simono}}$HKUST-1 (Figure S8). Besides, the binding energy of the silicone specie was shifted by 0.2 eV, suggesting the existence of electronic interaction at the interface between the deposited silicone shield and the $_{\text{mono}}$HKUST-1 (Figure S8).

Text S12. Discussion on thermal stability. Traditionally, thermal desorption at the GC inlet requires a temperature of at least 250 °C for the complete desorption of PAHs from a SPME fiber. Thus, thermal stability is a prerequisite for the material if it were to be used *via* a GC-MS system.[4,6–8] When the thermogravimetric analysis (TGA) experiments were conducted, HKUST-1 (*i.e.,* $_{\text{Simono}}$HKUST-1 and $_{\text{mono}}$HKUST-1) and ZIF-8 (*i.e.,* $_{\text{mono}}$ZIF-8 and $_{\text{powd}}$ZIF-8) turned out to be capable of withstanding a temperature of at least 320 °C (Figure S9) and 500 °C (Figure S10), respectively.

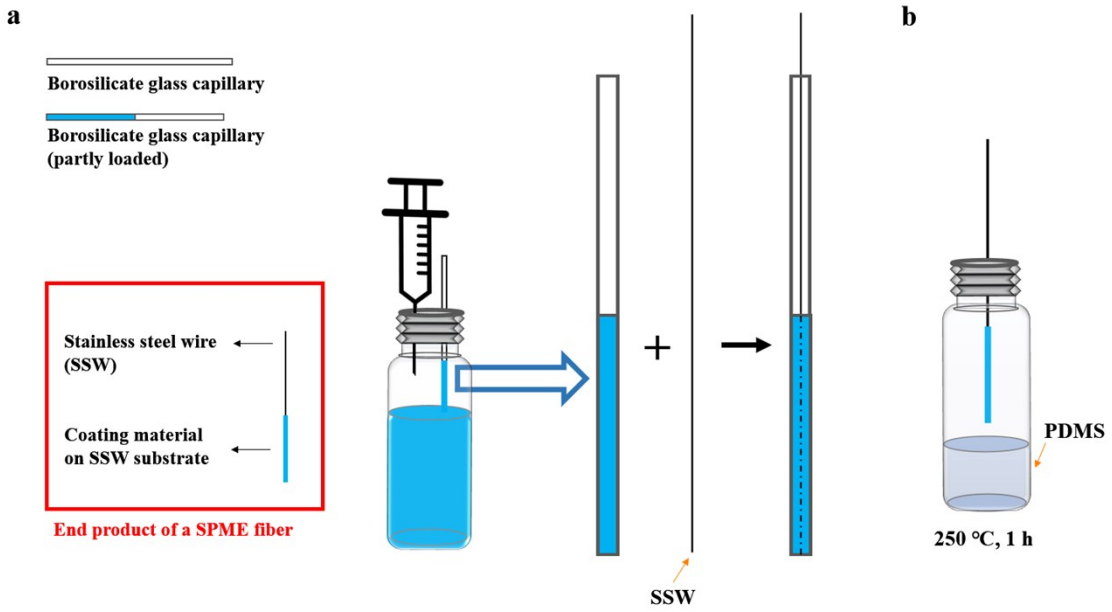

Scheme S1. Fabrication of the $_{Simono}$HKSUT-1 cylindrical coating. (a) Preparation of the $_{mono}$HKUST-1 coating. The material was pumped into the borosilicate glass capillary *via* pressure introduced by the syringe. Then the loaded capillary was placed at 25 °C for 24 h to go through a slow drying process to yield the cylindrical $_{mono}$HKUST-1 on the surface of the SWW. After that, the capillary was removed with great care using a tweezer. The vial was sealed with a septum-lined cap to create an air-tight environment. The inset in the red rectangle illustrated the end product of a SPME fiber. (b) The $_{mono}$HKUST-1 coating was later heated together with a PDMS stamp in a vial to yield the $_{Simono}$HKUST-1 fiber. The polymer cap septum was replaced with a tin foil for its thermal robustness.

a

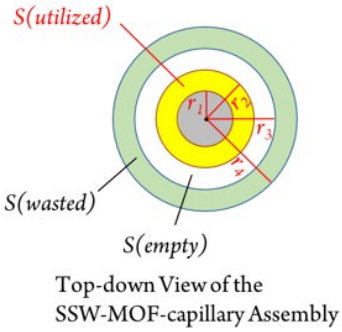

Top-down View of the SSW-MOF-capillary Assembly

$$V_{AUR} = \frac{V(utilized)}{V(utilized) + V(wasted)} \times 100\%$$

$$V = S \times h$$

$$S = \pi \times r^2$$

$$r_1 = \frac{127}{2}\mu m$$

$$r_2 = (\frac{127}{2} + 3)\mu m$$

$$r_3 = (\frac{250}{2} - 3)\mu m$$

$$r_4 = \frac{250}{2}\mu m$$

$$h = 1\ cm$$

b

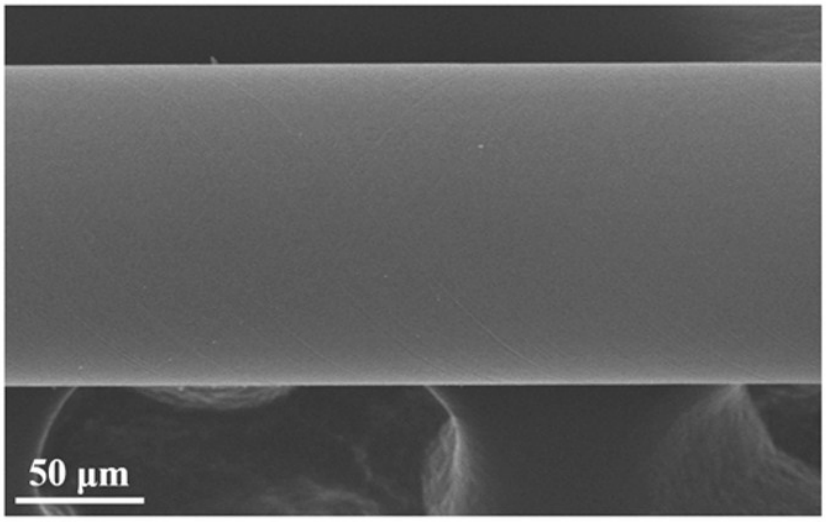

Figure S1. (a) Illustration of the calculation of atomic utilization ratio (AUR) which was represented by the ratio of the volume of the utilized $_{mono}$HKUST-1 to that of the total $_{mono}$HKUST-1 within the capillary (*i.e.,* V_{AUR}). r_1 was the radius of the SSW; r_2 was the radius of the $_{mono}$HKUST-1-coated SSW; r_3 was the distance from the center of the circle to the inner wall of the $_{mono}$HKUST-1-coated capillary; r_4 was the inner radius of a blank capillary. The yellow area represents the $_{mono}$HKUST-1 coating adhering to the SSW substrate (*i.e.,* the utilized MOFs); the green area represents the $_{mono}$HKUST-1 coating adhering to the capillary (*i.e.,* the wasted MOFs); the white area represents the empty space that appeared after the $_{mono}$HKUST-1 coatings were formed. Assuming that there coexisted an equal-thickness (*i.e.,* 3-µm-thick) $_{mono}$HKUST-1 coating adhering to the inner surface of the capillary (I.D. 250 µm), V_{AUR} was calculated to be *c.a.* 34.3%. In actual scenarios, because the MOFs might prefer adhering to the alloy substrates to adhering to borosilicate glass capillaries, the real V_{AUR} should be higher than 34.3%. (b) SEM image of a clean SSW. Note that the diameter was *c.a.* 127 µm. The coating thickness of the $_{mono}$HKUST-1 coating was 133 µm. Subtracting from this the diameter of the clean SSW (*i.e.,* 127 µm) and divided by 2, the thickness of the coating was calculated to be 3 µm. Similarly, the thickness of the $_{powd}$HKUST-1 coating was calculated to be 12 µm.

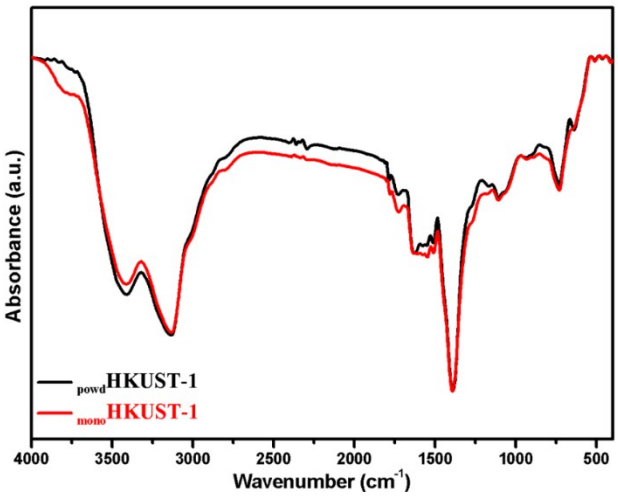

Figure S2. FT-IR of $_{powd}$HKUST-1 (black solid line) and $_{mono}$HKUST-1 (red solid line).

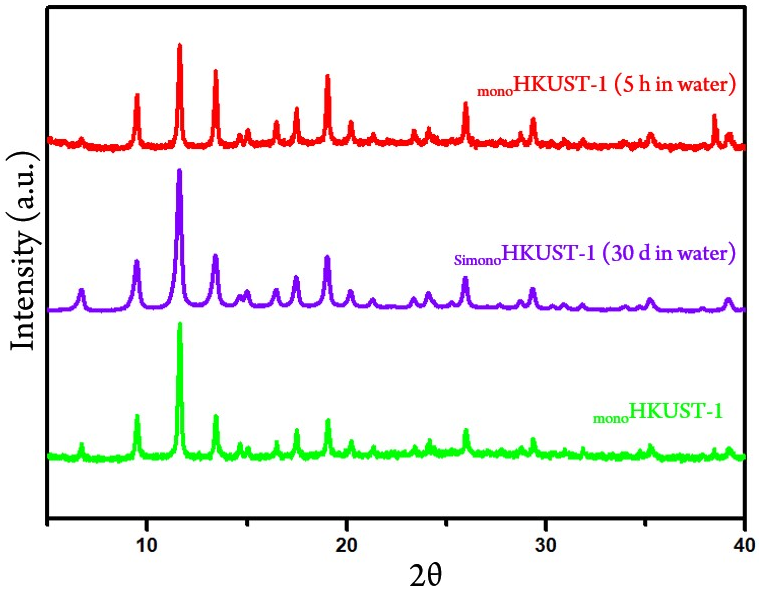

Figure S3. PXRD patterns of water-treated $_{mono}$HKUST-1 (soaked in water for 5 hours, red solid line), water-treated $_{Simono}$HKUST-1 (soaked in water for 30 days, violet solid line) and $_{mono}$HKUST-1 (green solid line).

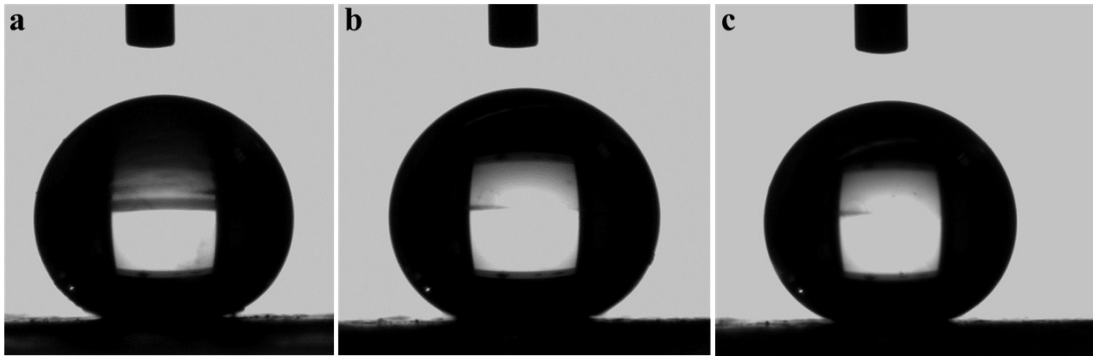

Figure S4. Water contact angle measurements of $_{Sipowd}$HKUST-1 (a); $_{Simono}$HKUST-1 before (b) and after (c) being immersed in water for 3 days followed by heating at 280 ℃ for 1h. It indicated the extra-durability of the ultra-thin silicone shield.

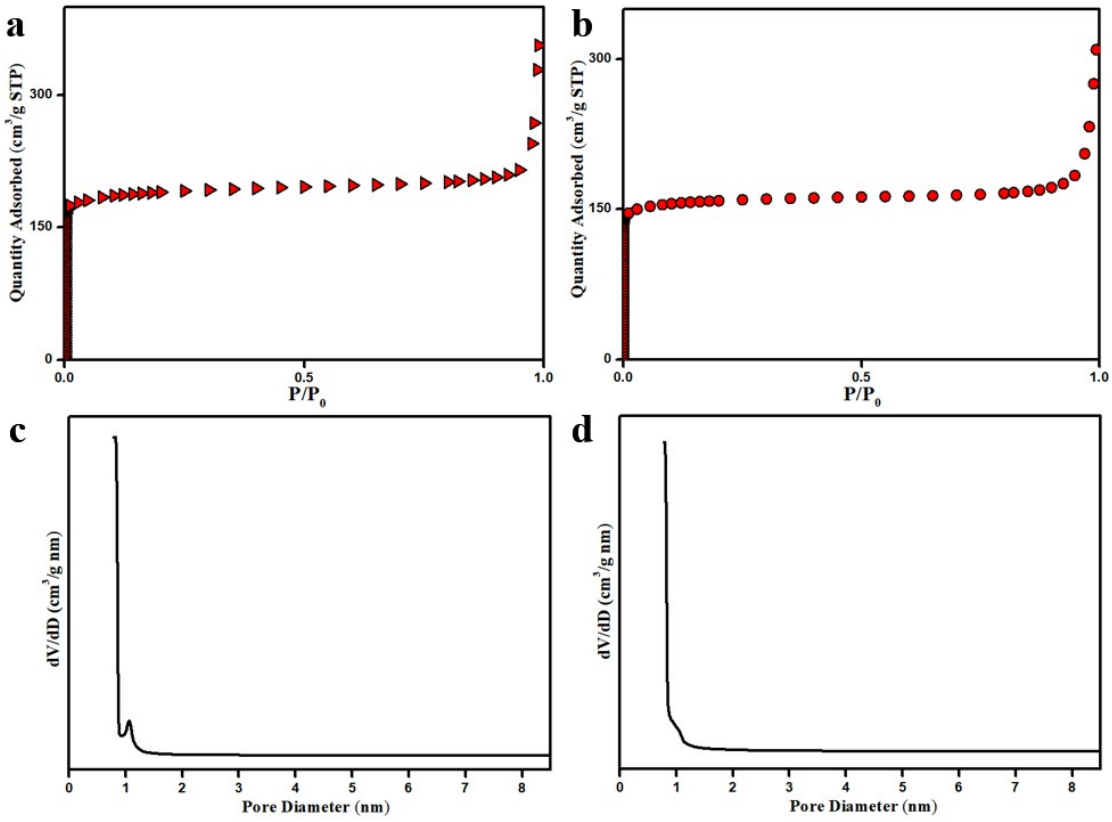

Figure S5. N_2 adsorption isotherm curves of $_{mono}$HKUST-1 (a) and $_{powd}$HKUST-1 (b). BET surface areas were 637.4 $m^2 g^{-1}$ and 757.6 $m^2 g^{-1}$ for $_{mono}$HKUST-1 and $_{powd}$HKUST-1, respectively. Using the Horvath-Kawazoe model, pore size distribution curves of $_{mono}$HKUST-1 (c) and $_{powd}$HKUST-1 (d) showed median pore width of 0.8642 nm and 0.9018 nm, respectively.

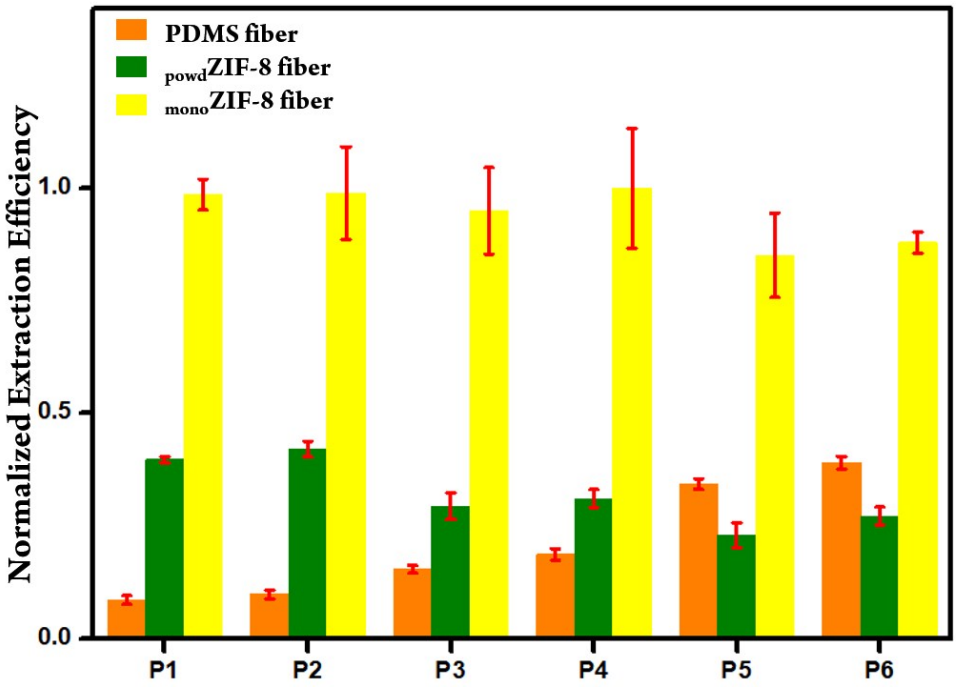

Figure S6. Extraction efficiency of six PAHs using the PDMS fiber (orange), the $_{powd}$ZIF-8 fiber (olive) and the $_{mono}$ZIF-8 fiber (yellow). Experimental conditions were 30 min (extraction time), 30 °C (extraction temperature) and 250 °C (desorption temperature).

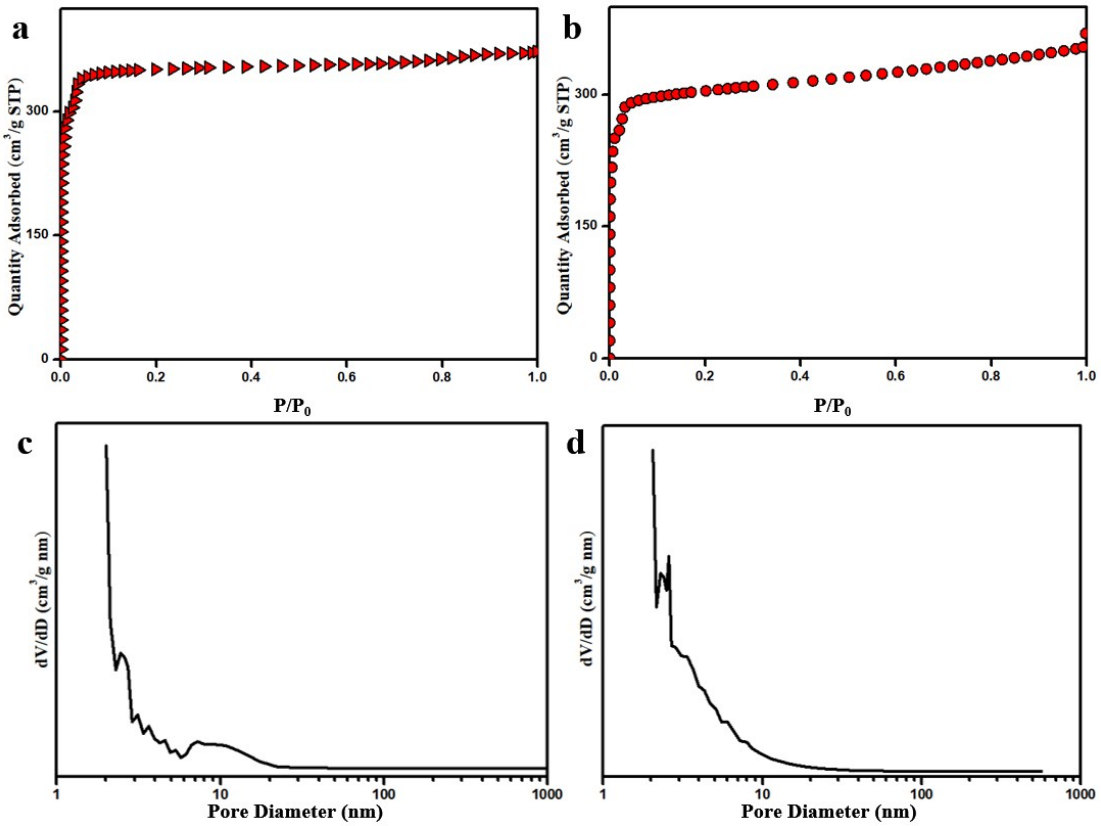

Figure S7. N_2 adsorption isotherm curves of $_{mono}$ZIF-8 (a) and $_{powd}$ZIF-8 (b). BET surface areas were 1403.8 $m^2 g^{-1}$ and 1199.8 $m^2 g^{-1}$ for $_{mono}$ZIF-8 and $_{powd}$ZIF-8, respectively. Pore size distribution curves of $_{mono}$ZIF-8 (c) and $_{powd}$ZIF-8 (d) showed pore diameters distributing predominantly around 2 nm.

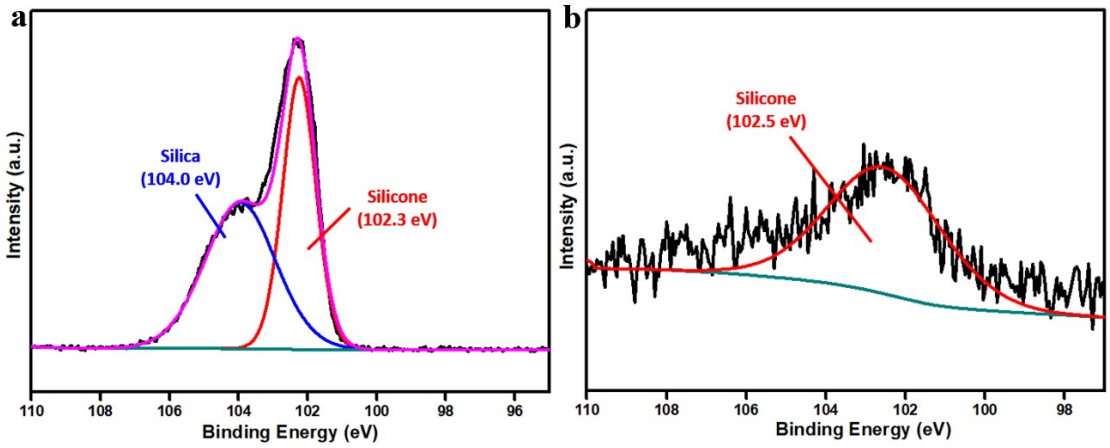

Figure S8. XPS spectra of Si2p from the silicone raw material (a) and the silicone deposited on the surface of $_{Simono}$HKUST-1 (b).

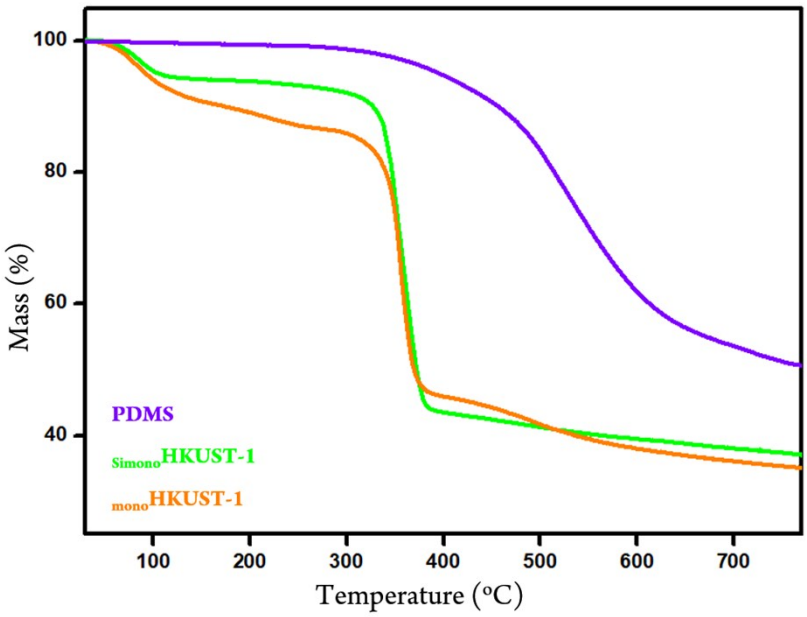

Figure S9. TG curves of $_{Simono}$HKUST-1 (green), $_{mono}$HKUST-1 (orange) and PDMS (violet).

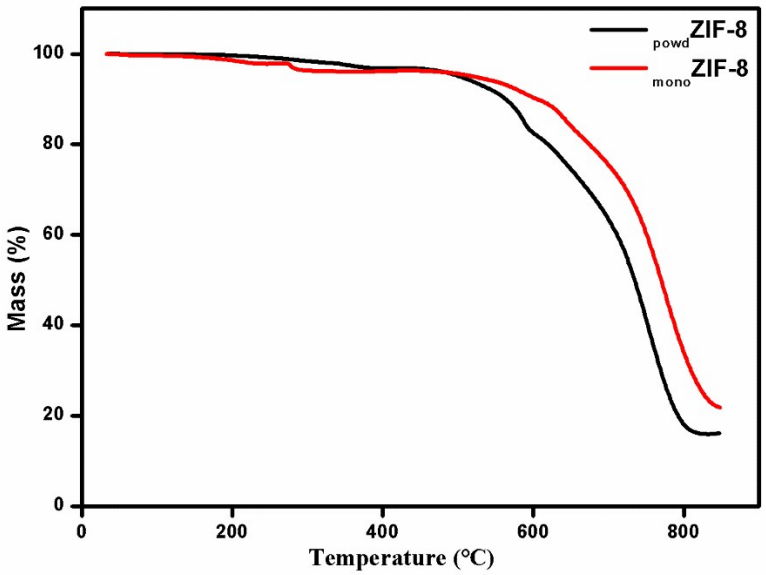

Figure S10. TG curves of $_{powd}$ZIF-8 and $_{mono}$ZIF-8. This result suggested that both samples were stable up to 500 °C, ready to withstand the high temperature at the GC-MS inlet during thermal desorption.

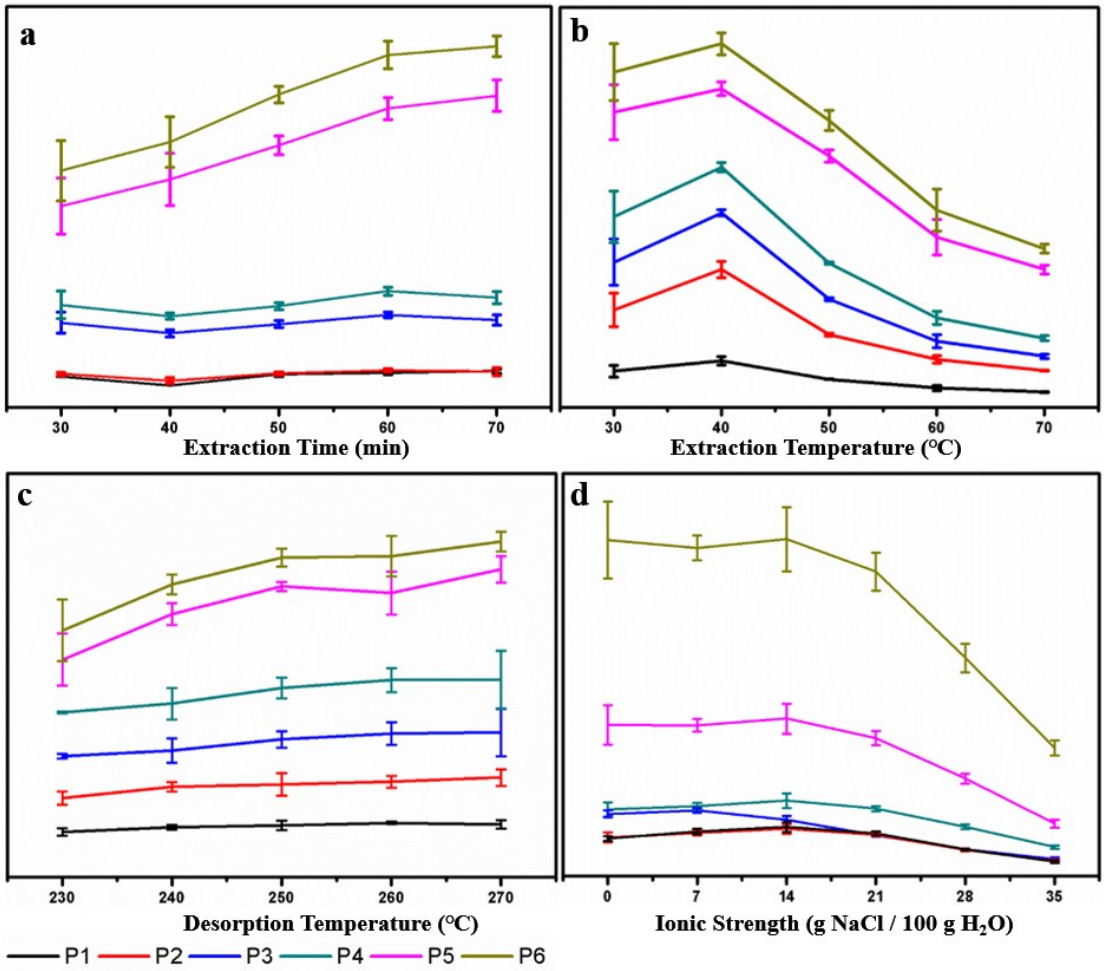

Figure S11. Optimization data of the experimental conditions including extraction time (a), extraction temperature (b), desorption temperature (c) and ionic strength (d).

Table S1. Mass percentage of $_{mono}$HKUST-1 and $_{powd}$HKUST-1 obtained *via* elemental analysis. The composition of the samples was almost identical to that of the theoretical hydrated HKUST-1, which was due to the adsorption of ambient moisture. Along with the PXRD data (Figure 2), it confirmed the successful synthesis of HKUST-1.

Sample	C (%)	H (%)	N (%)
$_{mono}$HKUST-1	30.14	2.51	0
$_{powd}$HKUST-1	30.18	2.41	0
Cal. HKUST-1	35.70	0.99	0
Cal. HKUST-1 (Hydrated)	30.29	2.52	0

Table S2. True density of $_{mono}$HKUST-1 and $_{powd}$HKUST-1. True density measurement excludes the volume of any open and closed pores, and is solely dependent on the constituent atoms of the material. Since $_{mono}$HKUST-1 and $_{powd}$HKUST-1 were identical in terms of elemental composition, it was not unexpected that their true densities data were basically the same.

Sample	ρ_1 (g cm^{-3})	ρ_2 (g cm^{-3})	ρ_3 (g cm^{-3})	$\bar{\rho}$ (g cm^{-3})
$_{mono}$HKUST-1	3.5484	3.3531	3.3266	3.4094
$_{powd}$HKUST-1	3.4252	3.4252	3.3783	3.4095

Table S3. BET areas, bulk density and volumetric BET areas of the as-synthesized $_{mono}$HKUST-1, $_{powd}$HKUST-1, $_{mono}$ZIF-8 and $_{powd}$ZIF-8.

Sample	BET area ($m^2 g^{-1}$)	ρ ($g cm^{-3}$)	Volumetric BET area ($m^2 cm^{-3}$)
$_{mono}$HKUST-1	637.4	1.08	688.4
$_{powd}$HKUST-1	757.6	0.43[a]	325.8
$_{mono}$ZIF-8	1403.8	1.10	1544.2
$_{powd}$ZIF-8	1199.8	0.35[b]	419.9

Note: [a] hand packing density[9]. [b] ZIF-8 density cited from BASF.

Table S4. Analytical figures of merit of the developed method using the $_{Simono}$HKUST-1 coating for the determination of target analytes.

Compound	Linear range (ng L^{-1})	R^2	LOD (ng L^{-1}, S/N = 3)	LOQ (ng L^{-1}, S/N = 10)	RSD (%)	
					Intra-fiber (n = 6)	Fiber to fiber (n = 3)
P1	5-10000	0.9941	0.99	3.30	4.0	13.7
P2	1-10000	0.9954	0.10	0.34	6.3	7.2
P3	1-10000	0.9930	0.17	0.57	6.0	9.3
P4	2-5000	0.9918	0.44	1.46	5.9	8.1
P5	1-5000	0.9965	0.12	0.40	4.2	12.1
P6	1-5000	0.9971	0.13	0.43	4.2	10.0

Table S5. Comparison of LODs of the developed method with those of reported ones. All the concentrations were in ng L^{-1}. The $_{Simono}$HKUST-1 coating is among the high-performance SPME fibers.

Analyte	$_{Simono}$HKUST-1- coated fiber (this work)	GNC-Co-coated fiber[10]	Cr(III) oxide-coated fiber[11]	Fe_2O_3 magnetic nanoparticle graphene[12]	3D-G fiber[13]	CBDCP-coated fiber[4]	Etched stainless steel wire fiber[7]
P1	0.99	-	-	16	-	2.10	260
P2	0.10	0.14	10	15	5.0	-	-
P3	0.17	2.47	10	13	4.0	0.29	420
P4	0.44	1.52	10	16	2.0	-	-
P5	0.12	0.88	-	10	2.0	0.11	580
P6	0.13	2.08	-	12	3.0	0.24	630

Table S6. Analytical results of rain water, LDC water and tap water samples, respectively. The spiked concentrations were 20 ng L^{-1}.

Compound	Rain water			LDC water			Tap water		
	Concentration (ng L^{-1})	Recovery (%)	RSD (%, n = 3)	Concentration (ng L^{-1})	Recovery (%)	RSD (%, n = 3)	Concentration (ng L^{-1})	Recovery (%)	RSD (%, n = 3)
P1	ND [a]	90.2	4.9	6.1	90.8	13.7	ND [a]	87.4	10.7
P2	3.5	81.0	6.2	4.3	103.9	7.2	3.2	104.5	5.6
P3	6.9	98.3	4.5	11.7	87.6	9.3	6.7	92.7	7.8
P4	2.5	86.5	5.1	14.8	82.3	8.1	ND [a]	88.0	11.1
P5	3.3	99.5	10.2	12.3	101.8	12.1	4.4	81.7	10.7
P6	3.9	99.1	10.3	11.0	112.4	10.0	3.4	87.2	9.9

[a] ND: not detected.

Table S7. Atomic percentage ratio of elements acquired from the XPS spectra of the $_{Simono}$HKSUT-1 and $_{Sipowd}$HKSUT-1. The elemental ratios of the samples were similar to that of the HKUST-1 rather than the hydrated HKSUT-1, suggesting the absence of hydrated H_2O in the composition, contrast to their moisture-sensitive counterparts. This is because of the water-repulsive property of the ultrathin silicone shield at the surface of the materials.

Sample	C : O	C : Cu	O : Cu
$_{Simono}$HKUST-1	1.66	6.29	3.79
$_{Sipowd}$HKUST-1	1.74	7.29	4.18
Cal. HKUST-1	1.5	6	4
Cal. HKUST-1 (Hydrated)	1	6	6

Table S8. Mass percentage of $_{mono}$ZIF-8 and $_{powd}$ZIF-8 obtained via elemental analysis. It suggested the successful synthesis of ZIF-8.

Sample	C (%)	H (%)	N (%)
$_{mono}$ZIF-8	41.82	4.27	24.49
$_{powd}$ZIF-8	41.86	4.19	24.50
Cal. ZIF-8	42.18	4.39	24.61

REFERENCE

1 T. Tian, Z. Zeng, D. Vulpe, M. E. Casco, G. Divitini, P. A. Midgley, J. Silvestre-Albero, J.-C. Tan, P. Z. Moghadam and D. Fairen-Jimenez, *Nat. Mater.*, 2017, **17**, 174–179.

2 M. Wiebcke, J. Cravillon, S. Münzer, S. J. Lohmeier, A. Feldhoff, K. Huber and S. Münzer, *Chem. Mater.*, 2009, **21**, 1410–1412.

3 T. Tian, J. Velazquez-Garcia, T. D. Bennett and D. Fairen-Jimenez, *J. Mater. Chem. A*, 2015, **3**, 2999–3005.

4 S. Wei, W. Lin, J. Xu, Y. Wang, S. Liu, F. Zhu, Y. Liu and G. Ouyang, *Anal. Chim. Acta*, 2017, **971**, 48–54.

5 J. Yuan, X. Liu, O. Akbulut, J. Hu, S. L. Suib, J. Kong and F. Stellacci, *Nat. Nanotechnol.*, 2008, **3**, 332–336.

6 R. Jiang, F. Zhu, T. Luan, Y. Tong, H. Liu, G. Ouyang and J. Pawliszyn, *J. Chromatogr. A*, 2009, **1216**, 4641–4647.

7 X. H.-L., L. Y., J. D.-Q. and Y. X.-P., *Anal. Chem.*, 2009, **81**, 4971–4977.

8 X. F. Chen, H. Zang, X. Wang, J. G. Cheng, R. S. Zhao, C. G. Cheng and X. Q. Lu, *Analyst*, 2012, **137**, 5411–5419.

9 Y. Peng, V. Krungleviciute, I. Eryazici, J. T. Hupp, O. K. Farha and T. Yildirim, *J. Am. Chem. Soc.*, 2013, **135**, 11887–11894.

10 C. Achten and W. Püttmann, *Environ. Sci. Technol.*, 2001, **35**, 1699–1699.

11 H. Liu, F. Ran, X. Wang, N. He and Y. Guo, *Microchim. Acta*, , DOI:10.1007/s00604-017-2535-2.

12 S. Zhang, W. Wu and Q. Zheng, *Anal. Methods*, 2015, **7**, 9587–9595.

13 S. Zhang, Z. Li, X. Yang, C. Wang and Z. Wang, *RSC Adv.*, 2015, **5**, 54329–54337.